Title

Endotype reversal as a novel strategy for screening drugs targeting familial Alzheimer's disease

Journal

Alzheimer's & Dementia, 18(11)

ISSN

1552-5260

Authors

Caldwell, Andrew B
Liu, Qing
Zhang, Can
et al.

Publication Date

2022-11-01

DOI

10.1002/alz.12553

Peer reviewed

Received: 1 February 2021 | Revised: 8 October 2021 | Accepted: 25 October 2021

DOI: 10.1002/alz.12553

Alzheimer's & Dementia®
THE JOURNAL OF THE ALZHEIMER'S ASSOCIATION

FEATURED ARTICLE

Endotype reversal as a novel strategy for screening drugs targeting familial Alzheimer's disease

Andrew B. Caldwell[1] | **Qing Liu**[2,3] | **Can Zhang**[4] | **Gary P. Schroth**[5] | **Douglas R. Galasko**[2] | **Kevin D. Rynearson**[2] | **Rudolph E. Tanzi**[4] | **Shauna H. Yuan**[2,6] | **Steven L. Wagner**[2,7] | **Shankar Subramaniam**[1,8,9,10]

[1] Department of Bioengineering, University of California, San Diego, La Jolla, California, USA

[2] Department of Neurosciences, University of California, San Diego, La Jolla, California, USA

[3] Department of Obstetrics, Gynecology, and Reproductive Sciences, University of California, San Diego, La Jolla, California 92093, USA

[4] Genetics and Aging Research Unit, Department of Neurology, Massachusetts General Hospital, Charlestown, Massachusetts, USA

[5] Illumina, Inc., San Diego, California, USA

[6] N. Bud Grossman Center for Memory Research and Care, Department of Neurology, University of Minnesota, Minneapolis, MN, USA; GRECC, Minneapolis VA Health Care System, Minneapolis, MN, USA

[7] VA San Diego Healthcare System, La Jolla, California, USA

[8] Department of Cellular and Molecular Medicine, University of California, San Diego, La Jolla, California, USA

[9] Department of Nanoengineering, University of California, San Diego, La Jolla, California, USA

[10] Department of Computer Science and Engineering, University of California, San Diego, La Jolla, California, USA

Correspondence
Shankar Subramaniam, Department of Bioengineering, University of California, San Diego, La Jolla, CA, 92093, USA.
Email: shankar@ucsd.edu

Funding information
Alzheimer's Association New Investigator Research Award, Grant/Award Number: NIRG-14-322164; NIH grants, Grant/Award Numbers: P50 AGO5131, U01 NS 074501-05, U01 AG048986, R01 LM012595, U01 CA198941, U01 DK097430, R01 DK109365, R01 HD084633, R01 HL108735; National Science Foundation grant, Grant/Award Number: STC CCF-0939370; Veterans Affairs RR&D, Grant/Award Number: 1I01RX002259; Cure Alzheimer's Fund

Abstract

While amyloid-β (Aβ) plaques are considered a hallmark of Alzheimer's disease, clinical trials focused on targeting gamma secretase, an enzyme involved in aberrant Aβ peptide production, have not led to amelioration of AD symptoms or synaptic dysregulation. Screening strategies based on mechanistic, multi-omics approaches that go beyond pathological readouts can aid in the evaluation of therapeutics. Using early-onset Alzheimer's (EOFAD) disease patient lineage *PSEN1*^{A246E} iPSC-derived neurons, we performed RNA-seq to characterize AD-associated endotypes, which are in turn used as a screening evaluation metric for two gamma secretase drugs, the inhibitor Semagacestat and the modulator BPN-15606. We demonstrate that drug treatment partially restores the neuronal state while concomitantly inhibiting cell cycle re-entry and dedifferentiation endotypes to different degrees depending on the mechanism of gamma secretase engagement. Our endotype-centric screening approach offers a new paradigm by which candidate AD therapeutics can be evaluated for their overall ability to reverse disease endotypes.

KEYWORDS
Alzheimer's disease, Alzheimer's therapy, disease endotypes, drug profiling, drug treatment, early-onset Alzheimer's disease, endotypes, familial Alzheimer's disease, gamma secretase, iPSC-derived neurons, iPSCs, presenilin1, PSEN1, RNA-seq

1 | NARRATIVE

1.1 | Contextual background

Alzheimer's disease (AD) is neurodegenerative form of dementia characterized by the progressive worsening of cognitive abilities. While early-onset familial AD (EOFAD), caused by mutations in the *PSEN1*, *PSEN2*, and *APP* genes, only accounts for at most 5% of all AD cases, it shares the hallmark pathology and symptoms with the sporadic, late-onset Alzheimer's disease (LOAD): misfolded β-amyloid (Aβ) accumulating as neuritic plaques and hyperphosphorylated tau aggregating as tangles combined with progressive memory loss and cognitive decline.[1] The presenilins (*PSEN1* and *PSEN2*) are the catalytic subunit of the gamma secretase protease complex, which ultimately proteolyzes Aβ peptides derived from the amyloid precursor protein (APP). The ratio of Aβ42, the Aβ peptide form with the highest pathogenic potential and most abundant in plaques,[2,3] to Aβ40 (i.e. the Aβ42/Aβ40 ratio) has been found to be consistently increased across over 200 familial AD-linked mutations.[4] Therapeutic compounds designed to treat AD by inhibiting gamma secretase enzymatic activity, such as Semagacestat and Avagacestat, successfully lowered Aβ peptides in both mice and humans but did not arrest disease progression, and in some patients, worsened symptoms.[5,6] The repeated failure of drugs targeting Aβ pathology challenged whether AD-associated pathology is the driver of disease etiology, or a consequence. A consistent observation in both AD model systems as well as postmortem patient brain samples is the loss of synaptic connectivity and activity; as a result, any hypothesis focused on deciphering the molecular mechanisms causing AD inception and progression alternative to the amyloid hypothesis must address and contextualize this loss of synaptic function. While historically the analysis of AD has focused on molecular readouts related to disease pathology—including Aβ peptide production and modifications of tau protein—the advent and popularization of *omics* approaches, particularly RNA-seq, ATAC-seq, and ChIP-seq, applied to the study of AD has actualized the ability to investigate the molecular mechanisms of disease onset and progression.

While studies on postmortem AD patient brain have provided a breadth of insight into disease progression, they offer only a snapshot at later stages of the disease. In contrast, human induced pluripotent stem cells (iPSCs) generated from EOFAD donor patient fibroblasts and differentiated into neurons (and other types of brain cells) offer the ability to investigate AD at the earliest stages of disease inception. Recent work by us and others have used a systems-level, multi-omics approach to characterize the molecular mechanisms of disease onset using EOFAD iPSC-derived neuron and LOAD induced neuron (iN) model systems, respectively. In our previous study, we generated iPSC-derived neurons from patients carrying four distinct *PSEN1* mutations and performed RNA-seq, ATAC-seq, and ChIP-seq to identify AD phenotype substates, or endotypes, defining transcriptional network modulation in order to ask the fundamental question: what are the molecular mechanisms which cause the inception and progression of AD? We demonstrated that the overarching endotypes associated with EOFAD—including activation of cell cycle reentry, non-ectoderm lineage dedifferentiation, and inflammation combined with the repression of neuronal lineage state specification and synaptic function—are driven by changes in the chromatin landscape.[7] The combined effect of activation of dedifferentiation programs coupled with loss of the mature neuronal lineage state cause EOFAD neurons to traverse the lineage landscape to a less-differentiated state. Mertens et al. applied a similar approach integrating RNA-seq and ATAC-seq performed on iNs generated from sporadic, late-onset AD patients, showing that modulation of these disease endotypes at the chromatin landscape level is a hallmark of LOAD as well.[8] Furthermore, recent network analysis of large LOAD patient cohorts such as the Religious Orders Study and Memory and Aging Project (ROSMAP) have identified disease modules related to synaptic loss, remodeling of neuronal lineage and the chromatin landscape, and inflammation.[9] As our iPSC-derived neuron model system and the characterized endotypes faithfully recapitulate human patient brain transcriptomic signatures associated with EOFAD, as well as sporadic LOAD modeled with iNs or observed in patient

RESEARCH IN CONTEXT

1. **Systematic review**: To date, there are no successful drugs that have been developed to target Alzheimer's disease (AD). This is primarily due to the absence of accurate animal models, the difficulty of assessing disease phenotypes in cellular and other model systems, and the absence of AD drug screening strategies. Recently, patient-derived, induced pluripotent stem cells differentiated into neurons have been used as model systems, making it possible to map cellular endotypes that reflect in vivo AD pathology.
2. **Interpretation**: Having developed AD-specific endotypes in familial AD cellular systems, we present here a novel strategy based on endotype screening. We apply this approach to assess the efficacy of two drugs which target the gamma secretase, the enzyme involved in aberrant Aβ-peptide cleavage and consequently amyloid plaques. We show the limitations of these drugs in their inability to address all disease endotypes.
3. **Future directions**: This manuscript proposes a new framework for drug screening in AD. In cellular model systems, we can assess if the mechanisms of pathology are addressed through redressing the disease endotypes. Such an assessment can be accomplished through examination of the expression phenotypes associated with aberrant mechanisms. This drug screening approach could be applied not only to the future evaluation of familial AD endotypes and AD drugs but expanded to sporadic AD and extended to other dementias–including Parkinson's disease, Huntington's disease, and ALS.

brains, it offers a new paradigm for evaluating candidate therapeutic compounds.

From previous work, it is evident that mutations in *PSEN1* have wide effects potentially unrelated to APP cleavage into Aβ peptides, potentially due to the hundreds of alternative gamma secretase substrates which may also undergo aberrant processing activity.[10] Therefore, targeting of gamma secretase activity could still potentially offer therapeutic benefit if a candidate drug were able to address not only aberrant Aβ peptide production, but molecular disease endotypes as well. In response to the failure of targeting gamma secretase via inhibition, members of our team developed a class of gamma secretase modulators, including the compound BPN-15606, which preferentially reduces Aβ42 peptide production while not affecting overall gamma secretase activity.[11,12] In the study presented here, we sought to evaluate the ability of the novel gamma secretase modulator (GSM), BPN-15606, in comparison with a previously developed gamma secretase inhibitor (GSI) Semagacestat, to transcriptionally revert disease endotypes towards a healthy control state. In addition to validating the novel screening strategy, we can delineate the distinct effects of the two drugs on endotype resolution.

1.2 | Study design and main results

Non-demented control (NDC) and *PSEN1*^{A246E} iPSCs were differentiated into CD184^{-}/CD44^{-} neurons as previously described.[7,13] As the *PSEN1*^{A246E} mutation causes aberrant processing of APP, and modulation of Aβ peptide dynamics has historically been a primary metric by which gamma secretase-targeting compounds are evaluated, we first treated NDC and *PSEN1*^{A246E} iPSC-derived neurons with the GSI Semagacestat and the GSM BPN-15606 and performed dose-response curves for APP proteolysis. As we previously reported, treatment with GSM selectively blocked Aβ42 and Aβ40 peptide production while Aβ38 peptide and overall Aβ production remained unaffected.[11] In contrast, treatment with GSI blocked all Aβ peptide types as well as total Aβ production. Interestingly, the GSM BPN-15606 has a preference for the EOFAD mutant form of gamma secretase, whereas the GSI Semagacestat has a preference for wild-type gamma secretase, as evidenced by IC_{50} measurements in NDC and *PSEN1*^{A246E} neurons. Next, we performed RNA-seq on NDC and *PSEN1*^{A246E} neurons treated with vehicle (DMSO), GSI, or GSM at highly efficacious concentrations (3.16 μM) for 72 hours. In concordance with our previous analysis of the *PSEN1*^{A246E} condition, differential expression, and enrichment analysis of the untreated *PSEN1*^{A246E} neurons relative to NDC neurons revealed four key AD-associated endotypes: activation of cell cycle reentry and dedifferentiation combined with repression of neuronal lineage definition and neuronal function. The combination of these disease endotypes drive neurons to a precursor-like, mixed lineage state, as evidenced by the activation of transcriptional regulators associated with alternative lineages (eg, mesendoderm lineage regulators, non-glutamatergic neuronal regulators) identified by multiple analysis approaches with unique underlying reference databases (ie, SwissRegulon, DoRothEA, and ENCODE-ChEA consensus databases). With establishing these four endotypes as molecular gene modules, we next sought to determine the extent to which these two drug compounds reversed the aberrant dysregulation of each endotype program back towards a healthy NDC state. This revealed that in addition to their differential modulation of proteolytic Aβ processing, the GSI Semagacestat and the GSM BPN-15606 have varying abilities to reverse each disease endotype in *PSEN1*^{A246E} neurons. We observed that GSM treatment results in a greater downregulation compared with GSI treatment of the cell cycle reentry and dedifferentiation endotypes activated in the *PSEN1*^{A246E} condition. For the neuron lineage and neuron function endotypes, the results were more nuanced, and the aberrant upregulation of early neuronal precursor state, due to activation of the transcriptional regulators OTX2 and RBPJ leading to upregulation of their corresponding target genes, is subsequently downregulated to a greater extent by GSM treatment compared to GSI; this comparative advantage of GSM treatment is also observed with respect to reversal of *PSEN1*^{A246E}-induced downregulation of late stage neuron and synaptic mitochondrial function mediated by NRF1. In contrast, GSI treatment resulted in a more significant reversal (activation) of late neuronal lineage commitment and synaptic function programs, which are comprised of mainly REST- and MYT1L-controlled genes.

1.3 | Study perspectives

In this study, we have demonstrated the utility of AD-associated transcriptional endotypes as metrics for evaluating candidate disease-modifying therapeutics. In concordance with our previous analysis of *PSEN1* mutant iPSC-derived neurons and patient brains, the hallmark mechanistic endotypes of familial AD characterized here using the *PSEN1*^{A246E} mutation all contribute to driving neurons to a dedifferentiated, mixed lineage state: activation of cell cycle and dedifferentiation endotypes combined with repression of neuronal lineage and synaptic function endotypes. We report that GSM treatment results in a greater reversal than GSI of the cell cycle and dedifferentiation endotypes, whereas GSM and GSI treatment both result in the reversal of the neuronal function endotype by targeting different transcriptional axes: GSM via activation of NRF1-controlled neuron mitochondrial energy genes and GSI via activation of REST-repressed and MYT1L-activated synaptic function genes. Our analysis of treatment efficacy at the endotype-level, especially when considering the effects on Notch-related gene expression, may aid in illustrating why inhibitors of gamma-secretase are not only ineffective at impeding but appear to accelerate the rate of disease progression. However, this analysis further suggests that even preferential alteration of gamma-secretase mediated Aβ peptide production alone may be insufficient at delaying overall disease progression. The suitability of experimental iPSC systems to test the efficacy of potential therapeutics has been investigated by us and others.[14,15] Here, we demonstrate that disease endotypes identified in our iPSC-derived neuron experimental system, reflective of processes that occur in EOFAD patient brains, not only can be used to evaluate the suitability of candidate therapeutic compounds and further characterize the mode by which they

reverse aberrant transcriptional regulatory mechanisms to drive neurons back to a more differentiated state, but also that drug compounds may have differential effects in healthy and AD model systems. Therefore, testing candidate drugs in model systems which faithfully recapitulate disease endotypes is imperative. Common disease-associated modules related to loss of synaptic function, loss of neuronal lineage state, cell cycle reentry, and dedifferentiation, which we have referred to here as endotypes, are molecular phenomena well-described in AD literature but also recently characterized by systems-level analysis of multi-omics data in EOFAD patient iPSC-neurons and postmortem brains,[7] sporadic AD iPSC-derived neurons and iNs,[8] and sporadic AD patient postmortem brains.[9] Our work here, strengthened by recent findings, demonstrates that these molecular disease endotypes represent common AD transcriptomically-defined states associated with disease onset and progression and collective targets for drug interventions.

The work we present here demonstrates the utility and potential of using AD endotype reversal as a screening metric for the evaluation of candidate drug compounds. This paves the way for addressing the following challenges and limitations in AD drug discovery research, which can be leveraged into potential advantages for future studies. The first limitation centers on the lack of diversity of AD subtypes: although this study focuses on EOFAD, specifically a hallmark *PSEN1* mutation—$PSEN1^{A246E}$ —which shares common disease endotypes observed in other *PSEN1* mutations in iPSC neurons, EOFAD brains, and LOAD iNs, there may be other endotypes associated with other forms of AD that are not captured in this mutation. The two drugs studied here specifically target gamma secretase cleavage activity, therefore a mutation in *PSEN1*, which are the most common drivers of EOFAD, was well suited to test the ability of the compounds to modulate aberrant gene programs. Future work is needed to identify alternative disease endotypes potentially associated with alternative forms of EOFAD and late-onset sporadic AD as well as those associated with other non-familial, early-onset sporadic forms of AD—which have not been well-represented in the large cohorts of AD patients studied thus far. However, the approach used for such future studies and the resulting insights gleaned may differ when focusing on forms of AD induced by familial mutations in *PSEN1*, *PSEN2*, and *APP* (ie, familial AD) versus those caused by the complex interplay between factors including gene polymorphisms (eg, *APOE*, *CLU*, *TREM2*), genetic background, sex, and age (ie, non-autosomal dominant AD [ADAD]).[16] Here, the model system used must be tailored to both the specific type of AD as well as the question being asked: while the iPSC-derived neuron system has been extensively used to model the highly penetrative EOFAD-causing familial mutations, an alternative model, such as iNs, may be more suitable to investigate the specific effects of sporadic AD risk factors. This is due to the fact that iPSC-derived cells likely undergo an age-related, epigenetic reset that may confound the study of non-ADAD types. An iN model system, which bypasses the epigenetic and chromatin reset via direct conversion from a fibroblast to a neuron, may be necessary in order to apply the endotype-centric screening approach to identify endotypes in non-ADAD subtypes, where the disease state may be more heterogeneous and dependent on a combination of age-related chromatin modifications or specific epigenetic configurations, genetic background, and risk factors such as *APOEε4*. It is important to note that the canonical sporadic AD risk factors may also play a role in the onset and progression of EOFAD caused by familial mutations, even though the interaction of these two disease axes is not well understood. In this study, donor lines were selected to limit potential confounding effects from these risk factors, namely by (1) selecting for non-*APOE4* carriers in both NDC (*APOEε2/3*) and $PSEN1^{A246E}$ (*APOEε3/3*) lines, (2) selecting an aged NDC donor (85 years) to reduce contribution of genetic background or aging that may potentiate towards AD, and (3) only using lines originating from male donors. Although neurons are potentially less affected by the *APOEε4* allele than astrocytes or microglia among brain cell types, there may be similar dysregulation of neuron differentiation induced by *APOEε4* relative to *APOEε3* in an isogenic background as observed for *PSEN1* mutations.[17] In contrast, the protective nature of the *APOEε2* is less well understood. Differential analysis of *APOEε2* allele carriers relative to *APOEε3* or *APOEε4* carriers in postmortem AD patient brains revealed increased mitochondrial function, unfolded protein response, and proteasomal degradation.[18] However, it is unclear whether this difference represents insight into the protective contributions of the *APOEε2* allele or an alternative path to a common sporadic AD endpoint. Interestingly, Lefterov et al. did not observe any differentially expressed genes between *APOEε3* and *APOEε4* carrier AD patients, highlighting the heterogeneous nature of sporadic AD, particularly when considering *APOEε4* status. Another recent study explored the *APOEε2* allele in an isogenic hiPSC-derived neuron model both in isolation and in conjunction with familial AD mutations in *PSEN1* and *APP*.[19] The authors demonstrated that although the *APOEε2* allele lowered Aβ production and Aβ42/Aβ40 ratios in $PSEN1^{A246E}$ mutant iPSC-derived neurons, it did not affect Aβ levels or ratios relative to the *APOEε3* allele. Another study in human patients demonstrated the protective effect of *APOEε2* in $PSEN1^{E280E}$ carriers, possibly due to maintained lipid processing, repression of synapse pruning by astrocytes, and proper innate immune regulation in microglia.[20,21] These studies highlight that alternative *APOE* alleles—either *APOEε2* or *APOEε4*—may be confounding factors when in combination with EOFAD (caused by familial mutations) or sporadic AD. While a baseline *APOEε2* carrier NDC, as used in this study, is less likely to affect the differential analysis than *APOEε4*, it is possible that contribution of *APOEε2* could exist along the same gene expression axis as disease endotypes; while literature evidence may point to *APOEε2* offering increased protection of disease endotypes, going beyond speculation would require specific experiments. On the one hand, in lieu of an isogenic background, an *APOEε2* control line could provide additional likelihood that it is truly non-demented—but it could also increase the apparent severity of disease endotypes in a familial AD mutation beyond what an *APOEε3/APOEε3* NDC baseline would provide.

Fortunately, the resources necessary to facilitate the study of familial AD mutations as well as AD risk factor genes in an isogenic genetic background are quickly expanding: the recently announced induced pluripotent stem cell Neurodegenerative Disease Initiative (iNDI) plans to make available iPSC lines capturing 134 different AD

and dementia-associated gene variants.[22] These AD iPSC lines will be generated using an isogenic background, which will enable the identification of disease endotypes caused by each mutation as well as directly compare the endotype-resolving ability of a candidate AD therapeutic in a given AD gene variant iPSC-derived neuron line relative to the isogenic background control.

The second limitation is centered on the potential limits of an iPSC-derived neuron or iN model system: there is increasing evidence that some mechanisms contributing to AD progression occur at the interplay between neurons and alternative brain cell types, including microglia and astrocytes. This could be addressed in two ways: firstly, by exploring familial AD mutations and AD risk genes using iPSC-derived microglia and astrocytes, particularly for risk genes which may have a larger disease effect in these cell types relative to neurons; and secondly, by using an iPSC-derived brain organoid model system to capture disease endotypes arising due to interactions between multiple brain cell types. Recent advances in the direct conversion of fibroblasts to astrocytes could aid in the exploration of AD risk factors where age-related epigenetic conformations may play a combinatorial role.[23,24] The third limitation is due to the short duration of drug treatment: iPSC-derived neurons do not generally survive for longer than 3 weeks in culture, so drug treatment regimens will necessarily be considerably shorter than in mouse model or human studies. The drug treatment duration could also be the reason that for both GSI and GSM treatments, as the cell cycle and dedifferentiation endotypes were modulated more substantially than the neuron lineage and function endotypes. However, iPSC-derived organoids have the potential to address this caveat as well: brain organoids can be grown for as long as a year in culture, offering the ability for longer treatment regimens which could accurately approximate human clinical trials. These potential weaknesses of the iPSC-derived neuron model system with respect to the study limitations can, in the right context, be leveraged into strengths; for one, the differentiation protocol from iPSCs to neurons is much more established, and easier to perform, than that of iNs or iPSC-derived organoids. Further, the differentiation process can be performed from the iPSC stage to NSC stage and NSCs frozen for long-term storage, allowing researchers to make large quantities of NSCs at one time and then continuing the differentiation process from NSCs to neurons at a later time for studying drug treatment. An endotype screening approach could be devised using a combination of two or more of these cell model systems in series: the first phase of drug screening could be done at a medium- to high-throughput level in iPSC-derived neurons, followed by a second phase for promising drugs which modulate endotypes in the previous phase in more complex iN and iPSC-derived organoid models.

1.4 | Conclusions and future recommendations

One key aspect of validating this endotype screening approach will be connecting the gene modules to physiological readouts related to each given endotype. For example, the cell cycle endotype, whereby gene expression signatures imply neuronal re-entry into the cell cycle, can be directly related to a measurement of the proportion of cells in the G_0-G_1, S, and G_2-M phases. Indeed, EOFAD iPSC-derived neurons from multiple *PSEN1* mutations demonstrate decreased proportion of cells in the G_0-G_1 and S phases and increased proportion of cells in the G_2-M phase of the cell cycle.[7] The reversal of these EOFAD trends by candidate drugs could be used as both validation of endotype screening as well as a method for further evaluation of each given drug.

The development of AD therapeutics presents several challenges. First, there is a need for understanding the combination of mechanisms that initiate and progress the pathology, preferably in a causal manner, to intervene in such a way that addresses the disease severity. Integrative, multiscale molecular measurements offer the scope to decipher such mechanisms. Next, we need model systems that are amenable to ex vivo experimental investigations while preserving the pathological mechanisms present in the human brain. Patient-derived transformable pluripotent cells offer the scope for developing such models, both at the level of individual cell types and brain organoid, with the latter involving vascularization of patient-specific organoids, for mechanistic investigations. Lastly, we need precise screens for validating the efficacy of therapeutics in alleviating the pathology. Endotype screens, such as the ones developed in this work, offer the opportunity to evaluate future drugs. Investigations at the nexus of multi-omics systems biology, stem cell technology, and high throughput screening approaches offer the best scope for addressing AD. In summary, the endotype screening approach which we have described here serves as a new paradigm for the evaluation of candidate therapeutics that can be easily expanded to alternative omics measurements (including quantitative measurements of chromatin dynamics via approaches like ATAC-seq, ChIP-seq, and HiC), transformed cell types (such as iNs and iPSC-derived organoids), as well as other neurodegenerative disease.

2 | CONSOLIDATED RESULTS

In our previous work, we used iPSC-derived neurons from EOFAD patients to identify disease-causal endotype mechanisms associated with AD and validated them in EOFAD postmortem patient brain.[7] Furthermore, we demonstrated that a gamma secretase modulator (GSM), BPN-15606, preferentially targets the plaque-forming peptides Aβ42 and Aβ40 and attenuates cognitive impairment in wild-type and PSAPP AD mouse models, respectively.[11,12] In light of this, we hypothesized that the GSM BPN-15606 may be effective at reversing dysregulated AD endotypes and sought to investigate drug efficacy in our clinically relevant EOFAD iPSC-derived neuron model. We selected the *PSEN1*^{A246E} EOFAD mutation to study endotype drug modulation and expanded our drug treatment to include a gamma secretase inhibitor (GSI) previously developed and tested by Eli Lilly, Semagacestat.

First, we treated NDC and *PSEN1*^{A246E} iPSC-derived neurons with vehicle (DMSO), GSI (Semagacestat), or GSM (BPN-15606), and measured Aβ peptide levels. While GSI treatment lowered levels of all Aβ peptide forms (Aβ42, Aβ40, Aβ38, and total Aβ), GSM treatment

preferentially lowered Aβ42 and Aβ40 levels while Aβ38 and total Aβ levels were unaffected. Interestingly, GSM treatment had a lower IC_{50} for Aβ42 and Aβ40 in *PSEN1*^{A246E} neurons compared with NDC, whereas the inverse was true for GSI treatment.

Next, we performed differential expression and enrichment analysis of NDC and *PSEN1*^{A246E} iPSC-derived neuron RNA-seq, revealing 1589 upregulated and 1676 downregulated genes in the *PSEN1*^{A246E} condition. Using a combination of ontology enrichment and Transcription Factor (TF) activity analysis, and in line with our previous study on *PSEN1*^{A246E} neurons, we observed five key endotypes associated with the disease state: upregulation of non-ectoderm dedifferentiation, cell cycle, and inflammation endotypes, and downregulation of neuronal lineage and synaptic function endotypes. We extended this same approach to *PSEN1*^{A246E} neurons treated with GSI or GSM relative to vehicle treatment (DMSO). Interestingly, GSM treatment resulted in a higher number of differentially expressed genes than GSI treatment, with 188 upregulated and 356 downregulated genes compared with 78 upregulated and 199 downregulated genes, respectively. Using ISMARA and DoRothEA TF activity analysis methods, we compared the ability of GSI and GSM treatment to modulate aberrantly activated or repressed TFs in the *PSEN1*^{A246E} condition for regulators related to the five key endotypes. This revealed that whereas GSM treatment has a stronger modulating effect on the TF activity of regulators related to the cell cycle and dedifferentiation endotypes, GSI has a stronger modulating effect on those related to neuronal lineage and synaptic function. This observed effect was sustained using classic hypergeometric and GSEA enrichment tests with reference ontology databases such as Hallmark, Reactome, and Gene Ontology: GSM treatment results in a higher number of genes significantly downregulated as well as a higher statistical significance of gene sets downregulated related to cell cycle and non-ectoderm lineage dedifferentiation compared to GSI treatment. The gamma secretase complex has numerous substrates in addition to APP, including Notch; the *PSEN1*^{A246E} mutation may contribute to aberrant Notch protein processing, resulting in altered expression of notch signaling genes and significant enrichment of Notch signaling gene sets as a whole. Interestingly, although GSM treatment retains normal Notch processing whereas GSI restricts notch processing, GSM has a more significant effect on downregulating the aberrant upregulation of Notch signaling genes in the *PSEN1*^{A246E} condition. With respect to the neuronal lineage and synaptic function endotypes, we observed different mechanisms by which GSI and GSM treatment reverses towards the non-demented control state. The dysregulation of the neuronal lineage state in the *PSEN1*^{A246E} condition is marked by concomitant upregulation of early-stage neuronal lineage commitment (controlled by regulators such as OTX2 and RBPJ) and downregulation of later stage neuronal lineage definition (controlled by regulators such as REST, MYT1L, and NRF1). Whereas GSM has a more significant effect on downregulating the aberrant upregulation of OTX2 and RBPJ (early commitment) as well as NRF1 (later stage in neuronal development and mitochondrial function) target genes, GSI treatment has a more significant effect on upregulating the aberrant downregulation of MYT1L and REST target genes (later stage in neuronal lineage specification and synaptic function).

3 | DETAILED METHODS AND RESULTS

3.1 | Methods

3.1.1 | iPSC line generation

NDC fibroblasts (Male; Age at biopsy: 85 years; APOE status: ε2/ε3) were derived from skin biopsies in accordance with UC San Diego IRB approval as previously described,[13] whereas *PSEN1*^{A246E} fibroblasts (Male; Age of onset: 50 years; Age at biopsy: 56 years; APOE status: ε3/ε3) were obtained commercially (Coriell Cat. AG06840). The generation and characterization of the iPSC lines were carried out as previously reported[25,26] from fibroblasts by retroviral transduction using the reprogramming factors *OCT4*, *SOX2*, *KLF4*, and *c-MYC*.

3.1.2 | Human neuron preparation

The protocol used for neuron preparation was previously described.[7,13] Briefly, PA6 cells were plated in a 10 cm dish and seeded with 100,000 cells iPSC next day. To enhance neural induction, cultures were treated with 500 ng/mL Noggin (R&D Systems) and 10 μM SB431542 (Tocris) for the first 6 days of differentiation. On day 12, neural stem cells (NSCs) were sorted using cell surface signature $CD24^+/CD184^+/CD44^-/CD271^-$.

NSCs were expanded in NSC growth medium (DMEM:F12+ Glutamax (Thermo Fisher Cat. 10565018), 1x B-27 (Thermo Fisher Cat. 17504044), 1x N-2 (Thermo Fisher Cat. 17502001), 1x Penicillin-Streptomycin (Thermo Fisher Cat. 15070063), and 20 ng/mL human bFGF-2 (BioPioneer Cat. HRP-0011)). At 80% confluence, the medium was changed to neuron differentiation medium (DMEM:F12+Glutamax, 1x B-27, 1x N-2, 1x Penicillin-Streptomycin) for 3 weeks of differentiation. After differentiation, the cultures were dissociated with Accutase (Sigma Cat. A6964). Cells were resuspended in 200 μL of iMag buffer (1x neural differentiation medium, 0.5 μM EDTA, 0.5% Bovine Serum Albumin) followed by incubation with PE Mouse Anti-Human CD184 and CD44 antibodies (BD Biosciences Cat. 561733 and 561858, respectively) for 15 minutes on ice in the dark. The mixture was washed with iMag buffer and subsequently incubated with anti-PE conjugated magnetic beads (BD Biosciences) for 30 minutes at room temperature. Magnetic bead separation was carried out for 8 minutes according to the manufacturer's protocol (BD Biosciences). The supernatant containing purified $CD184^-/CD44^-$ neurons was then removed and spun down for downstream applications.

3.1.3 | Compounds

The novel GSM BPN-15606, (*S*)-*N*-(1-(4-fluorophenyl)ethyl)-6-(6-methoxy-5-(4-methyl-1*H*-imidazol-1-yl)yridine-2-yl)-4-methylpyridazin-3-amine, was prepared at Albany Molecular Research Inc. (Albany NY) using methods previously reported.[27] The pharmacological and

toxicological properties of the GSM BPN-15606 have been previously described.[11,12] The GSI Semagacestat, *N*-[*N*-(3,5-difluorophenacetyl)-*L*-alanyl]-*S*-phenylglycine t-butyl ester, was purchased from Sigma-Aldrich (Millipore Sigma, Cat. 425386-60-3).

3.1.4 | RNA sequencing

iPSC-derived neurons were grown as described and treated with either the vehicle DMSO (0.01% v/v), the GSI Semagacestat, or the GSM BPN-15606 for 72 hours at a concentration of 3.16μM as described previously.[28] Total RNA from purified human NDC (biological replicates, DMSO $n = 3$) and $PSEN1^{A246E}$ (biological replicates, DMSO $n = 3$; Semagacestat $n = 3$; BPN-15606 $n = 3$) iPSC-derived neurons was prepared using Rneasy Plus Micro Kit (Qiagen Cat. 74034) according to the manufacturer's protocol. Libraries were prepared for RNA-seq using the TruSeq Stranded Total RNA Library prep kit (Illumina, Cat. RS-122-2303) by the Ribo-Zero ribosomal RNA reduction method (Illumina). Samples were sequenced at the UC San Diego Institute for Genomics Center sequencing core on an Illumina HiSeq4000 generating Paired-End, 75 bp reads with an average of 100 million reads per sample (Illumina, Cat. FC-410-1001).

3.1.5 | Data processing and differential expression analysis

Raw RNA-seq data was uploaded into Illumina's BaseSpace Sequence Hub, a cloud-based computing environment, for data processing. Sample read quality was assessed using the FastQC 1.0.0 program (one NDC sample was deselected for poor input RNA and read quality). Read mapping to the human genome (UCSC hg19) was performed using TopHat2 v2.0.7[29] and BowTie v0.12.9 within the TopHat Alignment v1.0 app on the Basespace platform, selecting the stranded and fusion calling features with the default parameters. Transcripts were assembled and abundances estimated using Cufflinks v.2.1.1[30] within the Cufflinks Assembly & DE v1.1 app on the Basespace platform, using the novel transcript assembly and adjusting transcript assembly for non-polyA selection. Differential expression analysis was performed with Cuffdiff v2.2 using the FPKM values generated from Cufflinks assembly within the Illumina Basespace Cufflinks Assembly & DE v1.1 app. Genes were deemed to have significant differential expression if they had a FDR-adjusted *P*-value of $< .05$. The $\log_2$ fold change ($\log_2$FC) and corresponding FDR *P*-value for $PSEN1^{A246E}$ (vehicle-treated, DMSO) were calculated relative to the NDC (vehicle-treated, DMSO) condition, while the $\log_2$FC and FDR *P*-value for Semagacestat or BPN-15606 treatment were calculated in relative to the untreated $PSEN1^{A246E}$ (DMSO) condition.

3.1.6 | Transcription factor activity analysis

TF activity analysis was performed using ISMARA[31] and DoRothEA.[32] For ISMARA analysis, fastq.gz RNA-seq files for all iPSC-derived neuron conditions were uploaded to ismara.unibas.ch for processing followed by sample average. In order to determine a directional z-score for each enriched motif identified, the z-score for each given motif was multiplied by the sign of the Pearson correlation between each motif and its target genes and the direction of change in expression for said target genes (ie, −1 for downregulated genes, +1 for upregulated genes). For motifs associated with miRNAs, qPCR expression in previous studies (miR-9, miR-124) or literature evidence (eg, miR-218) was used to determine a positive of negative correlation with gene targets of the given motif. For DoRothEA analysis, gene expression signatures were ranked by the $-\log_{10}$ of the FDR-adjusted *P*-value multiplied by the sign of the $\log_2$FC. TF activity analysis was performed using the *msviper* function in the *viper*[33] R package with the DoRothEA C regulon network.

3.1.7 | Gene set enrichment analysis

Gene Set Enrichment and Pathway Analysis for RNA-seq was performed using the *fgseamultilevel* function in the *fgsea*[34] R package with two TF-gene target databases, ENCODE-ChEA Consensus from Enrichr,[35,36] incorporating the consensus genes targets identified for 104 TFs from the Encyclopedia of DNA Elements (ENCODE) project[37] and Chip-X Enrichment Analysis (ChEA) datasets, and ReMap,[38] as well as two ontological databases, Gene Ontology-Biological Process (GOBP)[39] and Hallmark Pathway.[40] For the weighted, directional *fgsea* statistical enrichment test, genes were ranked by the $-\log_{10}$ of the FDR-adjusted *P*-value multiplied by the sign of the $\log_2$FC. When redundant gene sets were similarly enriched (gene sets corresponding to analogous biological processes), the gene set with the higher FDR q-value was presented.

Disease endotype gene lists were generated using published gene-set terms; for the cell cycle endotype, the Reactome: Cell cycle, Hallmark: G2-M phase, Hallmark: E2F targets, and ENCODE-ChEA Consensus: FOXM1 targets gene lists were used; for the dedifferentiation endotype, the Hallmark: EMT and the dbEMT v1.0[41] gene lists were used; for the neuron lineage endotype, the Reactome: Neuronal system, GOBP: Neuron differentiation, SOX11 target genes,[42] and RBPJ target genes[43]; for the synaptic function endotype, the Reactome: Neuronal system, GOBP: Synaptic Signaling, ENCODE-ChEA Consensus: REST target genes, and MYT1L target genes.[44,45] Genes occurring in multiple endotype lists were assigned to primary endotypes and removed from others using TF-gene target information and literature evidence.

3.1.8 | Cell-based Notch proteolytic processing assays

Human neuroblastoma (SH-SY5Y) cells stably overexpressing the human APP_{751} isoform (H4-APP751 cells) were transfected with Myc-tagged Notch (NΔED) construct and then treated with Semagacestat, BPN-15606, or DMSO (vehicle) at a variety of concentrations by serial dilution for an additional 24 hours. Cells were harvested 48 hours

post-transfection, and cell lysates were prepared and analyzed by western blotting for levels of NICD using an anti-Myc rabbit polyclonal antibody (Cell Signaling Cat. 2278) at a 1:1000 dilution and for levels of β-Actin using an anti-β-Actin mouse monoclonal antibody (Thermo Fisher Scientific Cat. 1295) at a 1:10000 dilution as detailed previously.[46] BPN-15606 Notch and β-Actin Western blots were previously reported.[11]

3.1.9 | Aβ assays and drug treatment

Sorted neurons were plated at 4.9×10^5 cells/cm^2 in a 96 well plate. Cells were treated with vehicle (DMSO), GSM BPN-15606 or GSI Semagacestat at various concentrations and assessed the IC_{50} by performing a 10-point dose response curves in DMSO (0.01% v/v) for 72 hours prior to the media collection as previously described.[28] MesoScale V-PLEX Aβ Peptide Panel 1 (6E10) Kit (MesoScale, Cat. K15200E-1) and Custom Human Total Aβ kit (MesoScale, Cat. N45CA-1) were used to assay Aβ peptides. IC_{50} and EC_{50} values represent the concentration in nM of compound required for reducing either Aβ42 or Aβ40 levels or increasing Aβ38 levels by 50% and are the mean of at least four determinations.

3.1.10 | Quantification and statistical analysis

GraphPad Prism v7.0b software was used for statistical analysis to calculate the non-linear regression for IC_{50} determination (Aβ drug treatment assays). All plots are presented in mean ± SD format.

3.1.11 | Data and software availability

The RNA-seq data generated in this study is available at the NCBI GEO under the accession GSE95673.

3.2 | Detailed results

3.2.1 | Aβ peptide quantification and IC_{50} in iPSC-derived neurons treated with GSI (Semagacestat) or GSM (BPN-15606)

In order to demonstrate and compare the ability of the GSI Semagacestat and the GSM BPN-15606 to modulate Aβ proteolysis in patient-derived neurons, NDC and *PSEN1*^{A246E} mutant iPSCs were generated and differentiated into neurons as previously described.[7,13] Both conditions were treated with GSI or GSM, measuring overall total Aβ levels and three key Aβ peptide alloforms (Aβ38, Aβ40, and Aβ42). Whereas the GSI Semagacestat lowered all forms of Aβ peptides, including Aβ38 and total Aβ, the GSM BPN-15606 selectively decreased secreted levels of the pathologically associated Aβ40 and Aβ42 peptides while maintaining total Aβ levels in both NDC and *PSEN1*^{A246E} neurons (Figure 1A–D).

3.2.2 | Differential gene expression and regulatory analysis in *PSEN1*^{A246E} iPSC-derived neurons relative to non-demented control

To establish the gene expression changes caused by the *PSEN1*^{A246E} mutation, we performed RNA-seq in both conditions, which demonstrated 3265 differentially expressed genes in *PSEN1*^{A246E} neurons relative to NDC (Figure 2A). In order to determine the TFs controlling these differentially expressed genes, we used two approaches to characterize TF activity: ISMARA,[31] a motif-centric TF activity analysis approach which identifies the TFs and miRNAs with motif activity change between *the PSEN1*^{A246E} and NDC neurons; and DoRothEA,[32] a TF-gene target-centric activity analysis approach which uses the *viper* activity inference algorithm with a curated regulon of TF-targets created from previously-published studies. In line with our previous analysis of *PSEN1*^{A246E} neurons,[7] the transcriptional regulators with the most significant activity change in the *PSEN1*^{A246E} condition by ISMARA analysis fell into four general disease-associated of disease-causal categories, termed here as endotypes: cell cycle (as evidenced by E2F family members),[47] dedifferentiation (including TEAD factors and PRRX2),[48,49] early neuron lineage commitment (RFX factors and RBPJ),[50,51] and synaptic function (REST and NRF1)[52,53] (Figure 2B). DoRothEA analysis identified the activity change of additional endotype-associated TFs, with an increase in activation of cell cycle (FOXM1, MYC) and dedifferentiation (SMAD3, TCF7L2) activators,[54 and a] decrease in neuron lineage (SOX11, ASCL1)[55,56] and synaptic function (MEIS1 and MEIS2) activators[57] (Figure 2C). Interestingly, DoRothEA analysis also identified the activation of hallmark inflammatory TFs, including NFκB, IRF, and STAT family members.[58,59] Next, we performed pre-ranked Gene Set Enrichment Analysis (GSEA) using *fgsea*[34,60] with two TF-target geneset databases: the ENCODE-ChEA Consensus (ECC) database from Enrichr[35,36] and our custom neural-associated TF database.[7] This approach similarly revealed significant enrichment with transcriptional activation of targets of TFs controlling cell cycle (E2F1, E2F6, FOXM1), dedifferentiation (YAP1/TAZ, NICD, SALL4),[61] and significant enrichment with transcriptional repression of targets of TFs controlling early neuron lineage (SOX11, RFX2) and neuron mitochondrial function (NRF1) (Figure 2D and E). Interestingly, targets activated by neuronal-promoting factor MYT1L were significantly enriched with decreased expression, whereas targets repressed by MYT1L were significantly enriched with increased expression, suggesting that the loss of the repressive and activation functions of MYT1L may contribute to both the activated dedifferentiation endotype (loss of MYT1L repression) and repressed neuronal endotypes (loss of MYT1L activation).[44,45] Next, we performed pre-ranked GSEA with *fgsea* using the Hallmark, Reactome, and Gene Ontology (GO) database, revealing significant enrichment with upregulation of genes related to cell cycle and

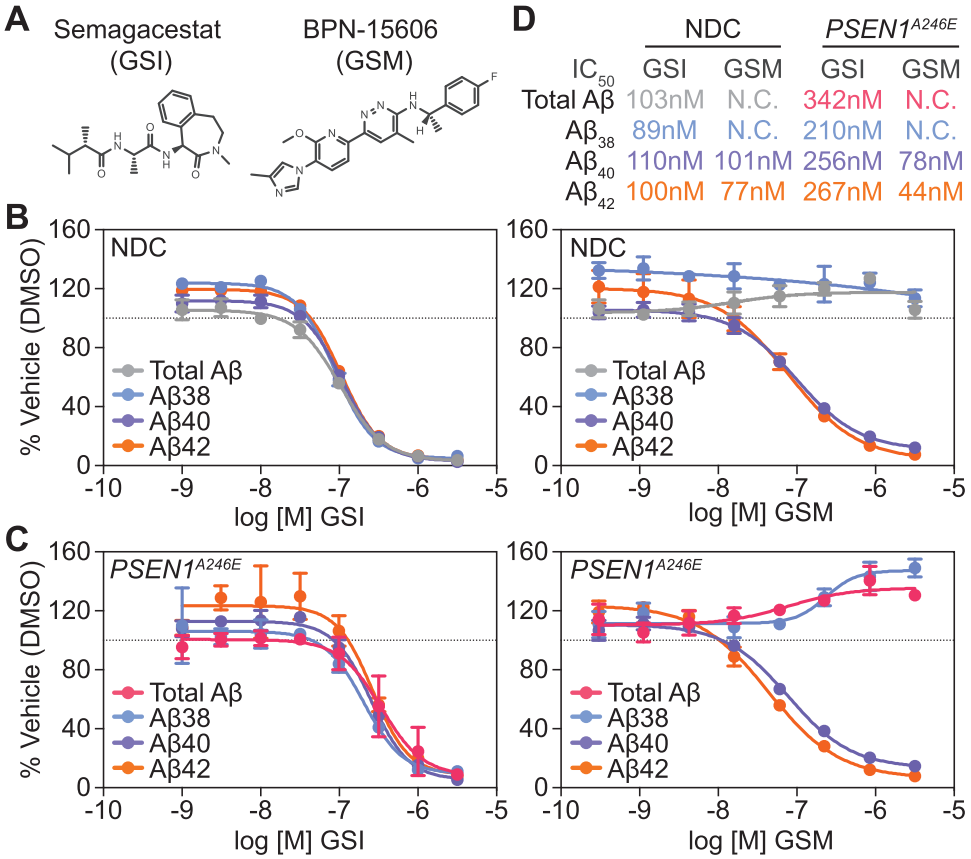

FIGURE 1 Gamma secretase-targeting compounds differentially modulate Aβ cleavage. (A) Molecular structure of the novel gamma secretase modulator (GSM) BPN-15606 and the gamma secretase inhibitor (GSI) Semagacestat. (B-C) Concentration response curves for the effects of the GSI Semagacestat and the GSM BPN-15606 in cell-based Aβ (Total Aβ, Aβ42, Aβ40, and Aβ38) peptide assays (Meso Scale) using conditioned media from (B) NDC and (C) *PSEN1*^{A246E} iPSC-derived neurons treated for 72 hours; biological replicates: $n = 3$; mean ± SD. (D) IC_{50} values representing the concentration in nM of compound required for reducing levels of either Total Aβ, Aβ42, Aβ40, or Aβ38 by 50%

non-ectoderm lineage dedifferentiation (mesendoderm lineage specification as evidenced by circulatory system-related development genesets), and significant enrichment with downregulation of gene related to neuron lineage specification and synaptic function, in alignment with the endotypes identified by TF activity analysis (Figure 2F and G).

3.2.3 | Differential gene expression and regulatory analysis in *PSEN1*^{A246E} iPSC-derived neurons treated with GSI (Semagacestat) or GSM (BPN-15606)

To determine whether drugs targeting gamma secretase would have transcriptional therapeutic reversal on the disease-associated endotypes and the overall transcriptional dysregulation in *PSEN1*^{A246E} neurons, we treated *PSEN1*^{A246E} neurons with either vehicle (DMSO), the GSI Semagacestat, or the GSM BPN-15606 and performed RNA-seq. This revealed 278 genes differentially expressed upon GSI treatment contrasted with 544 genes differentially expressed upon GSM treatment, with a greater number of downregulated DEGs in both treatment conditions (Figure 3A and B). Interestingly, the two treatment conditions shared substantial DEG overlap for genes upregulated in the *PSEN1*^{A246E} condition relative to NDC and subsequently downregulated upon Semagacestat or BPN-15606 treatment relative to vehicle treatment in *PSEN1*^{A246E} neurons, but modest DEG similarity for genes downregulated or not differentially expressed in the *PSEN1*^{A246E} condition relative to NDC (Figure 3C). In order to determine whether these unique DEGs are indicative of differential mechanisms between the two compounds, and further characterize the transcriptional modulation at the TF activity and endotype level, we again performed ISMARA and DoRothEA analysis. Interestingly, both GSI and GSM treatment caused an activity change reversal for endotype-associated TFs with significant activity change in *PSEN1*^{A246E} neurons by ISMARA analysis (Figure 3D). For neuronal endotype TFs, GSI treatment resulted in a greater activity loss for REST, whereas GSM treatment resulted in a greater activity gain for NRF1. The modulation of endotype-associated TF activity was similarly observed for GSI and GSM treatments by DoRothEA analysis, albeit with a different trend; GSM treatment resulted in a greater overall repression of cell cycle and dedifferentiation associated TFs activated in the *PSEN1*^{A246E} condition relative to

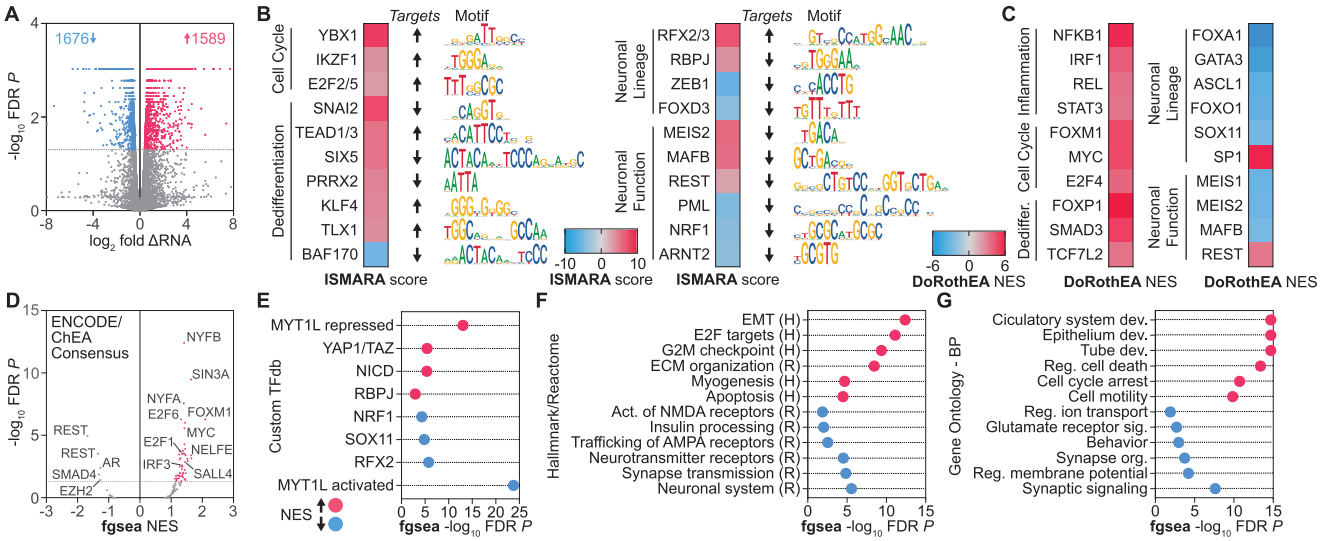

FIGURE 2 RNA-seq in *PSEN1*^{A246E} neurons identifies disease endotypes. (A) RNA-seq volcano plot of differentially expressed genes (DEGs) in *PSEN1*^{A246E} iPSC-derived neurons relative to NDC with a False Discovery Rate (FDR) adjusted *P*-value < .05. (B-C) Transcription Factors (TFs) with predicted significant activity change in *PSEN1*^{A246E} neurons by (B) ISMARA motif analysis (based on z-score, TF-gene Pearson correlation, and average gene target expression change) or (C) DoRothEA TF-gene target analysis (based on normalized enrichment score), curated into key modulated disease-associated endotypes. ISMARA average target gene expression change indicated by up (increasing relative to NDC) or down (decreasing relative to NDC) arrows. (D-E) Ranked TF-target enrichment in *PSEN1*^{A246E} neurons using the (D) ENCODE-ChEA Consensus TF database or (E) custom-defined list of neuronal associated TF-gene targets by the *fgsea* multilevel enrichment test. (F-G) Ranked enrichment analysis of *PSEN1*^{A246E} neuron gene expression signature using the (F) Hallmark and Reactome databases or (G) Gene Ontology–Biological Process (GOBP) by the *fgsea* multilevel enrichment test

NDC, whereas GSI treatment led to a greater activation of neuronal lineage associated TFs repressed in the *PSEN1*^{A246E} condition (Figure 3E). Given that our previously generated neuron associated TF-gene target gene set list was useful for the identification of key dysregulated TFs in *PSEN1*^{A246E} neurons, we again perform pre-ranked *fgsea* using this list for GSI- and GSM-treated cells. This approach demonstrated that GSI and GSM treatment similarly downregulate the YAP1/TAZ transcriptional axis of dedifferentiation, however only GSM treatment has a significant effect on alternative dedifferentiation axes driven by Notch or SOX9 activation (Figure 3F). Similarly, GSM treatment uniquely targets the aberrant upregulation of early neuronal lineage state activators OTX2 and RBPJ. Surprisingly, GSI and GSM treatment similarly represses the MYT1L-repressed targets aberrantly upregulated in *PSEN1*^{A246E}, but GSI, and not GSM, treatment leads to the activation of MYT1L-activated targets aberrantly downregulated in *PSEN1*^{A246E}. As both GSI and GSM treatment both had a larger number of significantly downregulated DEGs, we next sought to identify the gene sets overrepresented amongst these genes. We performed hypergeometric enrichment of downregulated DEGs following GSI or GSM treatment using the Hallmark and GOBP gene set libraries, revealing significant enrichment of cell cycle (Cell cycle, G_2-M checkpoint, and E2F targets) and dedifferentiation (EMT, Notch signaling, cardiovascular, and blood vessel development) gene sets in both treatment conditions (Figure 3G and H). Further, GSM treatment downregulated a substantially higher number of genes driving cell cycle re-entry and dedifferentiation compared to GSI treatment (Figure S1A and B). Next, we expanded the enrichment approach to pre-ranked enrichment using *fgsea* with the Hallmark, Reactome, and GOBP gene set libraries. By this approach as well, gene sets related to the cell cycle and dedifferentiation endotypes were significantly downregulated by GSI and GSM treatment, however this downregulation effect was statistically more significant for the GSM treatment condition compared with GSI (Figure 3K and L). As notch signaling pathways enrichment was reversed by both GSI and GSM treatment, and Semagacestat was previously found to inhibit Notch cleavage,[6] we assayed Notch proteolysis following GSI and GSM treatment. This revealed that while Semagacestat (GSI) treatment inhibited Notch protein cleavage into NICD, BPN-15606 (GSM) treatment allowed for normal Notch processing (Figure 3I). Despite this difference in modulation of gamma secretase-mediated Notch cleavage by the two drugs, GSM treatment resulted in a greater statistically significant downregulation of the Notch signaling geneset as well as a more substantial $\log_2$FC downregulation of discrete Notch pathway member genes (Figure 3J). Interestingly, the Reactome gene set Amyloid fibril formation was upregulated in the *PSEN1*^{A246E} condition relative to NDC and subsequently downregulated following GSI or GSM treatment in *PSEN1*^{A246E} neurons, with a stronger enrichment with gene downregulation following GSM treatment. Finally, while *fgsea* enrichment in the *PSEN1*^{A246E} condition relative to NDC revealed the enrichment with downregulated gene expression of neuronal function genesets, such as synaptic vesicle-mediated transmission, we did not observe these types of gene sets enriched following GSM treatment, but did observe synaptic function associated gene sets enriched with upregulation following GSI treatment.

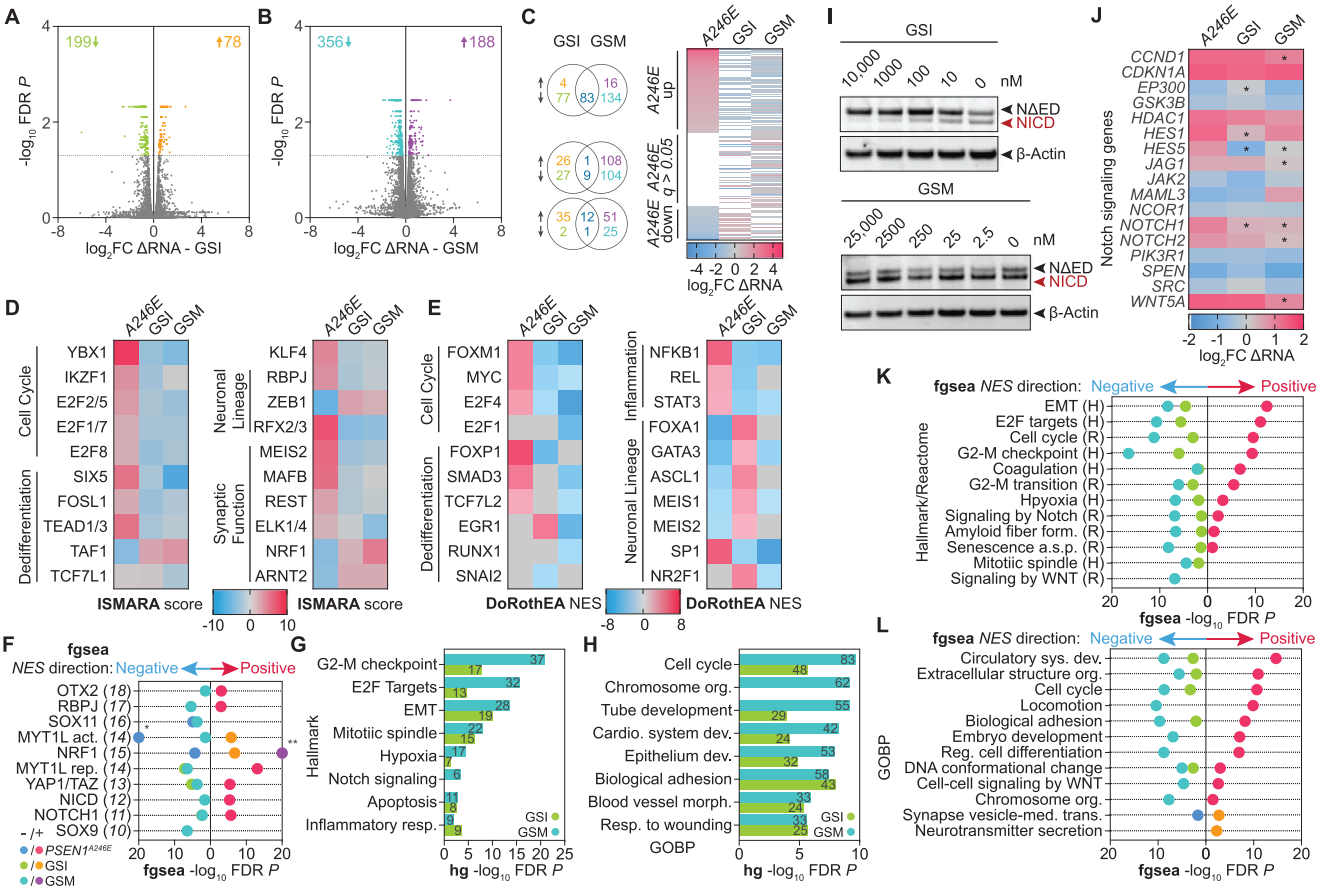

FIGURE 3 Semagacestat and BPN-15606 differentially modulate cell cycle, dedifferentiation, neuron lineage, and synaptic function disease endotypes. (A-B) RNA-seq volcano plot of DEGs in *PSEN1*^{A246E} neurons treated with (A) GSI or (B) GSM relative to vehicle (DMSO) treated *PSEN1*^{A246E} neurons with a FDR adjusted *P*-value < .05. (C) Heatmap and Venn diagrams of genes modulated by GSI or GSM treatment in *PSEN1*^{A246E} neurons; *PSEN1*^{A246E} condition relative to NDC; GSI and GSM treatment in *PSEN1*^{A246E} neurons relative to untreated condition. (D-E) TF activity change modulated by GSI or GSM treatment in *PSEN1*^{A246E} neurons by (D) ISMARA motif analysis or (E) DoRothEA TF-gene target analysis, curated into key disease-associated endotypes. (F) Ranked TF-target enrichment by the *fgsea* multilevel enrichment test in *psen1*^{A246E} neurons either untreated (DMSO) or treated with GSI or GSM using a custom-defined list of neuronal associated TF-gene targets. * > 20 -log$_{10}$ FDR *P*-value; ** > 75 -log$_{10}$ FDR *P*-value. (G-H) Hypergeometric enrichment of downregulated DEGs in GSI- or GSM-treated *PSEN1*^{A246E} neurons relative to untreated *PSEN1*^{A246E} neurons using the (G) Hallmark or (H) GOBP gene set databases. (I) Representative Western blot for Notch protein and *β*-Actin in BPN-15606- or Semagacestat-treated H4-APP751 cells expressing Myc-tagged Notch (NΔED). (J) log$_2$FC differential expression of Notch signaling genes in *PSEN1*^{A246E} neurons treated with vehicle (DMSO), GSI, or GSM relative to NDC neurons; * indicates the gene is differentially expressed relative to the untreated *PSEN1*^{A246E} condition. (K-L) Ranked enrichment analysis of gene expression signatures in *PSEN1*^{A246E} neurons treated with GSI or GSM relative to untreated *PSEN1*^{A246E} neurons or untreated *PSEN1*^{A246E} neurons relative to NDC neurons using the (K) Hallmark and Reactome databases or (L) Gene Ontology–Biological Process (GOBP) by the *fgsea* multilevel enrichment test

3.2.4 | Endotype transcriptional reversal in *PSEN1*^{A246E} iPSC-derived neurons treated with GSI (Semagacestat) or GSM (BPN-15606)

To investigate the network connectivity of the four disease endotypes modulated by Semagacestat or BPN-15606 treatment, we used StringDB and TF-gene target databases generated from previously-published ChIP-seq and siRNA expression data to generate PPI and TF-gene network modules based on the DEGs and key transcriptional regulators enriched for each endotype function with associated gene expression signatures for each treatment condition (DMSO, GSI, or GSM) in *PSEN1*^{A246E} neurons relative to NDC (Figure 4A–D). Across the four endotypes, GSM treatment resulted in a greater number of *PSEN1*^{A246E}-upregulated genes significantly downregulated; the median expression of all genes within each endotype generally followed this trend, with GSM treatment leading to a greater median overall gene expression decrease. In contrast, while GSI treatment resulted in the same number of upregulated DEGs that were *PSEN1*^{A246E}-downregulated for the cell cycle and dedifferentiation endotypes as GSM, it generated a greater number of upregulated DEGs for the neuron lineage and synaptic function endotypes. Further, the median expression increase of all *PSEN1*^{A246E}-downregulated DEGs for each endotype was higher for GSI treatment. In summary, these results demonstrate that Alzheimer's disease-causal endotypes are sensitive to reversal by gamma secretase-targeting therapeutics and further establishes the utility of AD-associated transcriptional

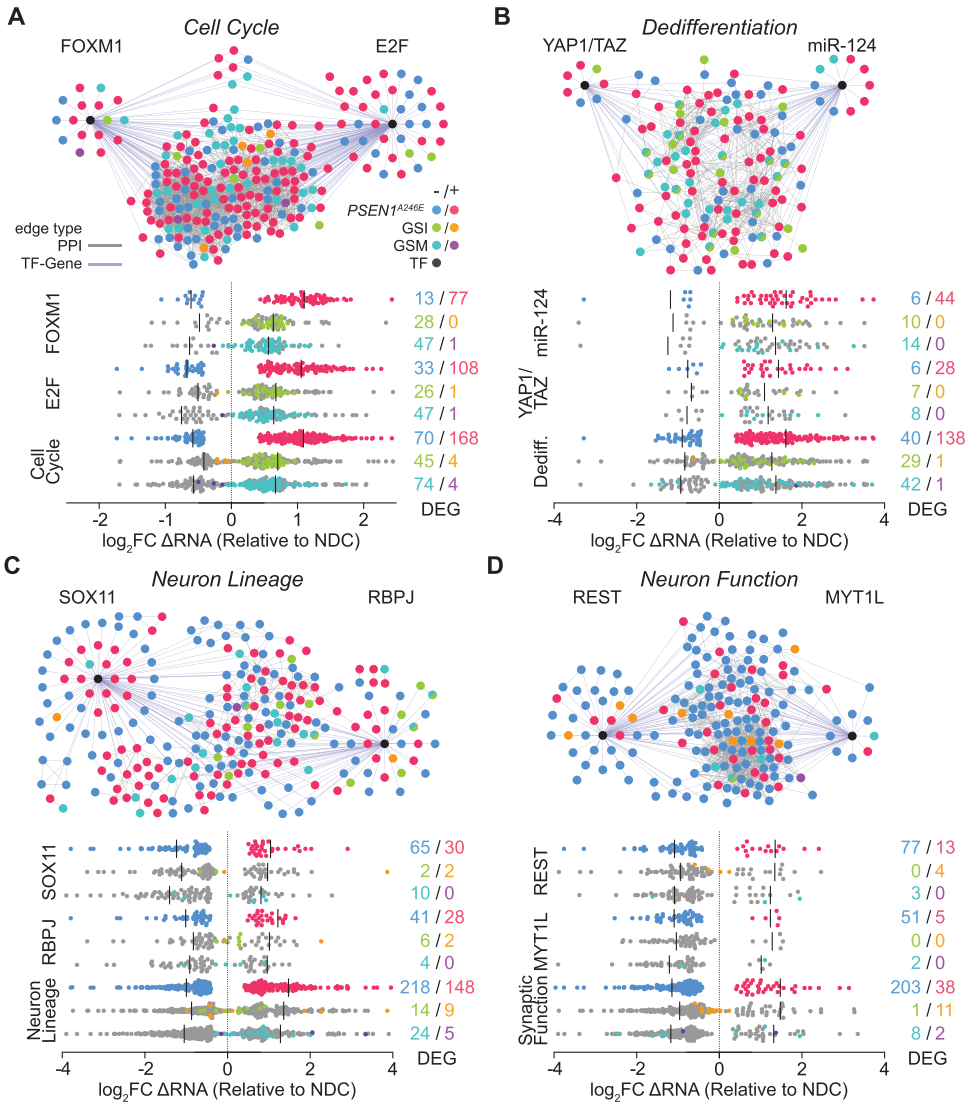

FIGURE 4 PPI and TF-gene target interactome networks illustrate the modulation of the four key *PSEN1*^{A246E} endotypes. (A-D) Combined PPI and TF-gene target networks, incorporating key enriched transcriptional regulators, with associated gene expression change in GSI- or GSM-treated *PSEN1*^{A246E} neurons or untreated *PSEN1*^{A246E} neurons for the four key endotypes: (A) Cell cycle, (B) Dedifferentiation, (C) Neuron lineage, and (D) Synaptic function

endotypes as a metric for evaluating candidate disease modulating therapeutics.

ACKNOWLEDGMENTS

This study was supported by the Alzheimer's Association New Investigator Research Award (NIRG-14-322164) to S.H.Y.; NIH grants P50 AGO5131 (D.R.G), U01 NS 074501-05 (S.L.W), U01 AG048986 (S.L.W), R01 LM012595 (S.S.), U01 CA198941 (S.S.), U01 DK097430 (S.S.), R01 DK109365 (S.S.), R01 HD084633 (S.S.), and R01 HL108735 (S.S.); the National Science Foundation grant STC CCF-0939370 (S.S.); the Joan and Irwin Jacobs Endowment (S.S.); the Cure Alzheimer's Fund (CAF) grants to S.L.W. and R.E.T.; and the Veterans Affairs RR&D 1I01RX002259 (S.L.W.). S.L.W. and S.S. also acknowledge a grant from the D.H. Chen Foundation. The contents do not represent the views of the U.S. Department of Veterans Affairs or the U.S. government.

AUTHOR CONTRIBUTIONS

Andrew B. Caldwell carried out the analysis of the RNA-seq experiments and wrote the manuscript with contributions to the Methods section from other authors. Andrew B. Caldwell and Shankar Subramaniam were involved in the characterization of the endotype modulation associated with drug treatment. Shauna H. Yuan was involved in the design of iPSC differentiation into neurons and the drug treatment experiments along with Steven L. Wagner. Qing Liu supervised by Shauna H. Yuan carried out the iPSC-neuron preparation, RNA isolation, and analysis of the Aβ assay data. Gary P. Schroth contributed to the RNA sequencing. Kevin D. Rynearson and Rudolph E. Tanzi were

involved along with Steven L. Wagner in the discovery and development of BPN-15606. Can Zhang performed the Notch experiments. Douglas R. Galasko was involved in part of the study design. Shankar Subramaniam and Steven L. Wagner were involved in the overall study design, analysis, and revisions of the manuscript.

FINANCIAL DISCLOSURE

Rudolph E. Tanzi is a shareholder of a privately held company (Neurogenetic Pharmaceuticals, Inc) that holds rights to an unrelated GSM currently in early clinical development. All other authors have no financial disclosures to state pertinent to this study.

ORCID

Andrew B. Caldwell https://orcid.org/0000-0002-2850-7677
Qing Liu https://orcid.org/0000-0002-8845-1417
Can Zhang https://orcid.org/0000-0002-4340-5118
Gary P. Schroth https://orcid.org/0000-0002-3055-056X
Douglas R. Galasko https://orcid.org/0000-0001-6195-3241
Kevin D. Rynearson https://orcid.org/0000-0002-6490-4792
Rudolph E. Tanzi https://orcid.org/0000-0002-7032-1454
Shauna H. Yuan https://orcid.org/0000-0003-4058-4146
Steven L. Wagner https://orcid.org/0000-0003-4674-9474
Shankar Subramaniam https://orcid.org/0000-0002-8059-4659

REFERENCES

1. Tanzi RE. The genetics of Alzheimer disease. *Cold Spring Harb Perspect Med*. 2012; 2: a006296.
2. Iwatsubo T, Odaka A, Suzuki N, Mizusawa H, Nukina N, Ihara Y. Visualization of A beta 42(43) and A beta 40 in senile plaques with end-specific A beta monoclonals: evidence that an initially deposited species is A beta 42(43). *Neuron*. 1994; 13: 45-53.
3. Tanzi RE, Bertram L. Twenty years of the Alzheimer's disease amyloid hypothesis: a genetic perspective. *Cell*. 2005; 120: 545-555.
4. Potter R, Patterson BW, Elbert DL, et al. Increased in vivo amyloid-β42 production, exchange, and loss in presenilin mutation carriers. *Sci Transl Med*. 2013; 5: 189ra77.
5. Coric V, van Dyck CH, Salloway S, et al. Safety and tolerability of the γ-secretase inhibitor avagacestat in a phase 2 study of mild to moderate Alzheimer disease. *Arch Neurol*. 2012; 69: 1430-1440.
6. De Strooper B. Lessons from a failed γ-secretase Alzheimer trial. *Cell*. 2014; 159: 721-726.
7. Caldwell AB, Liu Q, Schroth GP, et al. Dedifferentiation and neuronal repression define familial Alzheimer's disease. *Sci Adv*. 2020; 6: eaba5933.
8. Mertens J, Herdy JR, Traxler L, et al. Age-dependent instability of mature neuronal fate in induced neurons from Alzheimer's patients. *Cell Stem Cell*. 2021;28:1533-1548.e6.
9. Neff RA, Wang M, Vatansever S, et al. Molecular subtyping of Alzheimer's disease using RNA sequencing data reveals novel mechanisms and targets. *Sci Adv*. 2021; 7: eabb5398.
10. Moehlmann T, Winkler E, Xia X, et al. Presenilin-1 mutations of leucine 166 equally affect the generation of the Notch and APP intracellular domains independent of their effect on Aβ42 production. *Proc Natl Acad Sci U S A*. 2002; 99: 8025-8030.
11. Wagner SL, Rynearson KD, Duddy SK, et al. Pharmacological and toxicological properties of the potent oral γ-secretase modulator BPN-15606. *J Pharmacol Exp Ther*. 2017; 362: 31-44.
12. Prikhodko O, Rynearson KD, Sekhon T, et al. The GSM BPN-15606 as a potential candidate for preventative therapy in Alzheimer's disease. *J Alzheimers Dis*. 2020; 73: 1541-1554.
13. Yuan SH, Martin J, Elia J, et al. Cell-surface marker signatures for the isolation of neural stem cells, glia and neurons derived from human pluripotent stem cells. *PLoS One*. 2011; 6: e17540.
14. van der Kant R, Langness VF, Herrera CM, et al. Cholesterol metabolism is a druggable axis that independently regulates tau and amyloid-β in iPSC-derived Alzheimer's disease neurons. *Cell Stem Cell*. 2019; 24: 363-375.e9.
15. Williams G, Gatt A, Clarke E, et al. Drug repurposing for Alzheimer's disease based on transcriptional profiling of human iPSC-derived cortical neurons. *Transl Psychiatry*. 2019; 9:220.
16. Penney J, Ralvenius WT, Tsai LH. Modeling Alzheimer's disease with iPSC-derived brain cells. *Mol Psychiatry*. 2020; 25: 148-167.
17. Lin YT, Seo J, Gao F, et al. APOE4 causes widespread molecular and cellular alterations associated with Alzheimer's disease phenotypes in human iPSC-derived brain cell types. *Neuron*. 2018; 98: 1141-1154.e7.
18. Lefterov I, Wolfe CM, Fitz NF, et al. APOE2 orchestrated differences in transcriptomic and lipidomic profiles of postmortem AD brain. *Alzheimers Res Ther*. 2019; 11: 113.
19. Brookhouser N, Raman S, Frisch C, Srinivasan G, Brafman DA. APOE2 mitigates disease-related phenotypes in an isogenic hiPSC-based model of Alzheimer's disease. *Mol Psychiatry*. 2021. https://doi.org/10.1038/s41380-021-01076-3
20. Vélez JI, Lopera F, Sepulveda-Falla D, et al. APOE*E2 allele delays age of onset in PSEN1 E280A Alzheimer's disease. *Mol Psychiatry*. 2016; 21: 916-924.
21. Li Z, Shue F, Zhao N, Shinohara M, Bu G. APOE2: protective mechanism and therapeutic implications for Alzheimer's disease. *Mol Neurodegener*. 2020; 15: 63.
22. Ramos DM, Skarnes WC, Singleton AB, Cookson MR, Ward ME. Tackling neurodegenerative diseases with genomic engineering: a new stem cell initiative from the NIH. *Neuron*. 2021; 109: 1080-1083.
23. Caiazzo M, Giannelli S, Valente P, et al. Direct conversion of fibroblasts into functional astrocytes by defined transcription factors. *Stem Cell Rep*. 2015; 4: 25-36.
24. Gatto N, Dos Santos Souza C, Shaw AC, et al. Directly converted astrocytes retain the ageing features of the donor fibroblasts and elucidate the astrocytic contribution to human CNS health and disease. *Aging Cell*. 2021; 20: e13281.
25. Liu GH, Barkho BZ, Ruiz S, et al. Recapitulation of premature ageing with iPSCs from Hutchinson-Gilford progeria syndrome. *Nature*. 2011; 472: 221-225.
26. Israel MA, Yuan SH, Bardy C, et al. Probing sporadic and familial Alzheimer's disease using induced pluripotent stem cells. *Nature*. 2012; 482: 216-220.
27. Wagner SL, Mobley WC, Tanzi RE, et al. Potent γ-secretase modulators. World Intellectual Property Organization patent WO/2016/070107. May 6, 2016.
28. Liu Q, Waltz S, Woodruff G, et al. Effect of Potent γ-Secretase Modulator in Human Neurons Derived From Multiple Presenilin 1–Induced Pluripotent Stem Cell Mutant Carriers. *JAMA Neurology*. 2014;71(12):1481. https://doi.org/10.1001/jamaneurol.2014.2482
29. Kim D, Pertea G, Trapnell C, Pimentel H, Kelley R, Salzberg SL. TopHat2: accurate alignment of transcriptomes in the presence of insertions, deletions and gene fusions. *Genome Biol*. 2013; 14: R36.
30. Trapnell C, Hendrickson DG, Sauvageau M, Goff L, Rinn JL, Pachter L. Differential analysis of gene regulation at transcript resolution with RNA-seq. *Nat Biotechnol*. 2013; 31: 46-53.
31. Balwierz PJ, Pachkov M, Arnold P, Gruber AJ, Zavolan M, van Nimwegen E. ISMARA: automated modeling of genomic signals as a democracy of regulatory motifs. *Genome Res*. 2014; 24: 869-884.

32. Garcia-Alonso L, Holland CH, Ibrahim MM, Turei D, Saez-Rodriguez J. Benchmark and integration of resources for the estimation of human transcription factor activities. *Genome Res*. 2019; 29: 1363-1375.
33. Alvarez MJ, Shen Y, Giorgi FM, et al. Functional characterization of somatic mutations in cancer using network-based inference of protein activity. *Nat Genet*. 2016; 48: 838-847.
34. Korotkevich G, Sukhov V, Sergushichev A. Fast gene set enrichment analysis. Preprint. Posted online October 22, 2019. BioRxiv 060012. https://doi.org/10.1101/060012
35. Chen EY, Tan CM, Kou Y, et al. Enrichr: interactive and collaborative HTML5 gene list enrichment analysis tool. *BMC Bioinformatics*. 2013; 14: 128.
36. Kuleshov MV, Jones MR, Rouillard AD, et al. Enrichr: a comprehensive gene set enrichment analysis web server 2016 update. *Nucleic Acids Res*. 2016; 44: W90-W97.
37. Sloan CA, Chan ET, Davidson JM, et al. ENCODE data at the ENCODE portal. *Nucleic Acids Res*. 2016; 44: D726-D732.
38. Chèneby J, Gheorghe M, Artufel M, Mathelier A, Ballester B. ReMap 2018: an updated atlas of regulatory regions from an integrative analysis of DNA-binding ChIP-seq experiments. *Nucleic Acids Res*. 2018; 46: D267-D275.
39. Ashburner M, Ball CA, Blake JA, et al. Gene Ontology: tool for the unification of biology. *Nat Genet*. 2000; 25: 25-29.
40. Croft D, O'Kelly G, Wu G, et al. Reactome: a database of reactions, pathways and biological processes. *Nucleic Acids Res*. 2011; 39: D691-D697.
41. Zhao M, Kong L, Liu Y, Qu H. dbEMT: an epithelial-mesenchymal transition associated gene resource. *Sci Rep*. 2015; 5: 11459.
42. Kuo PY, Leshchenko VV, Fazzari MJ, et al. High-resolution chromatin immunoprecipitation (ChIP) sequencing reveals novel binding targets and prognostic role for SOX11 in mantle cell lymphoma. *Oncogene*. 2015; 34: 1231-1240.
43. Borromeo MD, Meredith DM, Castro DS, et al. A transcription factor network specifying inhibitory versus excitatory neurons in the dorsal spinal cord. *Development*. 2014; 141: 2803-2812.
44. Mall M, Kareta MS, Chanda S, et al. Myt1l safeguards neuronal identity by actively repressing many non-neuronal fates. *Nature*. 2017; 544: 245-249.
45. Yokoyama A, Igarashi K, Sato T, et al. Identification of myelin transcription factor 1 (MyT1) as a subunit of the neural cell type-specific lysine-specific demethylase 1 (LSD1) complex. *J Biol Chem*. 2014; 289: 18152-18162.
46. Wagner SL, Zhang C, Cheng S, et al. Soluble γ-secretase modulators selectively inhibit the production of the 42-amino acid amyloid β peptide variant and augment the production of multiple carboxy-truncated amyloid β species. *Biochemistry*. 2014;53(4):702-713. https://doi.org/10.1021/bi401537v
47. Sadasivam S, DeCaprio JA. The DREAM complex: master coordinator of cell cycle dependent gene expression. *Nat Rev Cancer*. 2013; 13: 585-595.
48. Lv ZD, Wang HB, Liu XP, et al. Silencing of Prrx2 inhibits the invasion and metastasis of breast cancer both in vitro and in vivo by reversing epithelial-mesenchymal transition. *Cell Physiol Biochem*. 2017; 42: 1847-1856.
49. Zhang H, Liu CY, Zha ZY, et al. TEAD transcription factors mediate the function of TAZ in cell growth and epithelial-mesenchymal transition. *J Biol Chem*. 2009; 284: 13355-13362.
50. Fujimoto M, Takagi Y, Muraki K, et al. RBP-J promotes neuronal differentiation and inhibits oligodendroglial development in adult neurogenesis. *Dev Biol*. 2009; 332: 339-350.
51. Sugiaman-Trapman D, Vitezic M, Jouhilahti EM, et al. Characterization of the human RFX transcription factor family by regulatory and target gene analysis. *BMC Genomics*. 2018; 19: 181.
52. Ballas N, Grunseich C, Lu DD, Speh JC, Mandel G. REST and its corepressors mediate plasticity of neuronal gene chromatin throughout neurogenesis. *Cell*. 2005; 121: 645-657.
53. Dhar SS, Wong-Riley MTT. Coupling of energy metabolism and synaptic transmission at the transcriptional level: role of nuclear respiratory factor 1 in regulating both cytochrome c oxidase and NMDA glutamate receptor subunit genes. *J Neurosci*. 2009; 29: 483-492.
54. Lamouille S, Xu J, Derynck R. Molecular mechanisms of epithelial–mesenchymal transition. *Nature Reviews Molecular Cell Biology*. 2014;15(3):178-196. https://doi.org/10.1038/nrm3758
55. Bergsland M, Werme M, Malewicz M, Perlmann T, Muhr J. The establishment of neuronal properties is controlled by Sox4 and Sox11. *Genes Dev*. 2006; 20: 3475-3486.
56. Park NI, Guilhamon P, Desai K, et al. ASCL1 reorganizes chromatin to direct neuronal fate and suppress tumorigenicity of glioblastoma stem cells. *Cell Stem Cell*. 2017; 21: 209-224.e7.
57. Agoston Z, Heine P, Brill MS, et al. Meis2 is a Pax6 co-factor in neurogenesis and dopaminergic periglomerular fate specification in the adult olfactory bulb. *Development*. 2014; 141: 28-38.
58. Honda K, Takaoka A, Taniguchi T. Type I inteferon gene induction by the interferon regulatory factor family of transcription factors. *Immunity*. 2006; 25: 349-360.
59. Shih VF, Tsui R, Caldwell A, Hoffmann A. A single NFκB system for both canonical and non-canonical signaling. *Cell Res*. 2011; 21: 86-102.
60. Subramanian A, Tamayo P, Mootha VK, et al. Gene set enrichment analysis: a knowledge-based approach for interpreting genome-wide expression profiles. *Proc Natl Acad Sci U S A*. 2005; 102: 15545-15550.
61. Liu L, Zhang J, Yang X, Fang C, Xu H, Xi X. SALL4 as an epithelial-mesenchymal transition and drug resistance inducer through the regulation of c-Myc in endometrial cancer. *PLoS One*. 2015; 10: e0138515.

SUPPORTING INFORMATION

Additional supporting information may be found in the online version of the article at the publisher's website.

How to cite this article: Caldwell AB, Liu Q, Zhang C, et al. Endotype reversal as a novel strategy for screening drugs targeting familial Alzheimer's disease. *Alzheimer's Dement*. 2022;18:2117–2130. https://doi.org/10.1002/alz.12553